Journal for ImmunoTherapy of Cancer

Expression of VISTA regulated via IFN-γ governs endogenous T-cell function and exhibits correlation with the efficacy of CD19 CAR-T cell treated B-malignant mice

Donghai Tang,[1] Li Zhao,[1] Fen Yan,[1] Chunxiao Ren,[1] Kailin Xu ,[1,2] Kai Zhao [1,2]

To cite: Tang D, Zhao L, Yan F, *et al*. Expression of VISTA regulated via IFN-γ governs endogenous T-cell function and exhibits correlation with the efficacy of CD19 CAR-T cell treated B-malignant mice. *Journal for ImmunoTherapy of Cancer* 2024;**12**:e008364. doi:10.1136/jitc-2023-008364

► Additional supplemental material is published online only. To view, please visit the journal online (https://doi.org/10.1136/jitc-2023-008364).

Accepted 30 May 2024

Check for updates

© Author(s) (or their employer(s)) 2024. Re-use permitted under CC BY-NC. No commercial re-use. See rights and permissions. Published by BMJ.

[1]Xuzhou Medical University, Xuzhou, Jiangsu, China
[2]Department of Hematology, Affiliated Hospital of Xuzhou Medical University, Xuzhou, Jiangsu, China

Correspondence to
Professor Kai Zhao; kainyzhao@163.com

Professor Kailin Xu; lihmd@163.com

ABSTRACT

Background Despite continuous improvements in the new target and construction of chimeric antigen receptor (CAR)-T, relapse remains a significant challenge following CAR-T therapy. Tumor microenvironment (TME) strongly correlates with the efficacy of CAR-T therapy. V-domain Ig suppressor of T-cell activation (VISTA), which exerts a multifaceted and controversial role in regulating the TME, acts not only as a ligand on antigen-presenting cells but also functions as a receptor on T cells. However, the characteristics and underlying mechanisms governing endogenous T-cell activation by VISTA, which are pivotal for reshaping the TME, remain incompletely elucidated.

Methods The immunocompetent B acute lymphoblastic leukemia (B-ALL), lymphoma, and melanoma murine models were employed to investigate the characteristics of endogenous T cells within the TME following CD19 and hCAIX CAR-T cell therapy, respectively. Furthermore, we examined the role of VISTA controlled by interferon (IFN)-γ signaling in regulating endogenous T-cell activation and functionality in B-ALL mice.

Results We demonstrated that the administration of CD19 CAR-T or hCAIX CAR-T cell therapy elicited augmented immune responses of endogenous T cells within the TME of B-ALL, lymphoma, and melanoma mice, thereby substantiating the efficacy of CAR-T cell efficacy. However, in the TME lacking IFN-γ signaling, VISTA levels remained elevated, resulting in attenuated cytotoxicity of endogenous T cells and reduced B-ALL recipient survival. Mice treated with CD19 CAR-T cells exhibited increased proportions of endogenous memory T cells during prolonged remission, which possessed the tumor-responsive capabilities to protect against B-ALL re-challenge. Compared with wild-type (WT) CAR-T treated mice, the administration of IFN-$\gamma^{-/-}$ CAR-T to both WT and IFN-$\gamma^{-/-}$ recipients resulted in a reduction in the numbers of endogenous $CD4^+$ and $CD8^+$ effectors, while exhibiting increased populations of naïve-like $CD4^+$ T and memory $CD8^+$ T cells. VISTA expression consistently remained elevated in resting or memory $CD4^+$ T cells, with distinct localization from programmed cell death protein-1 (PD-1) expressing T subsets. Blocking the VISTA signal enhanced dendritic cell-induced proliferation and cytokine production by syngeneic T cells.

Conclusion Our findings confirm that endogenous T-cell activation and functionality are regulated by VISTA, which is associated with the therapeutic efficiency of CAR-T and provides a promising therapeutic strategy for relapse cases in CAR-T therapy.

WHAT IS ALREADY KNOWN ON THIS TOPIC

⇒ The interaction between chimeric antigen receptor (CAR)-T cells and components of the tumor microenvironment has a significant impact on the efficacy of CAR-T cell therapy, necessitating further elucidation of the characteristics and regulation of endogenous T cells.

WHAT THIS STUDY ADDS

⇒ Enhanced immune activation, accompanied by downregulated expression of V-domain Ig suppressor of T-cell activation (VISTA) on endogenous T cell, was observed following CAR-T treatment in both hematologic B-malignant and melanoma mice. The tumor-responsive endogenous T cells were regulated by the interferon-γ/VISTA signaling pathway and could be stimulated by dendritic cells, thereby conferring protection against B acute lymphoblastic leukemia re-challenges and enhancing CD19 CAR-T efficacy.

HOW THIS STUDY MIGHT AFFECT RESEARCH, PRACTICE OR POLICY

⇒ These data substantiate the rationale for targeting VISTA to enhance endogenous T-cell response, thereby augmenting the efficacy of CAR-T therapy.

INTRODUCTION

CD19 chimeric antigen receptor (CAR) T cells offered a promising therapeutic strategy for the treatment of refractory and relapsed (R/R) B acute lymphoblastic leukemia (B-ALL).[1 2] The US Food and Drug Administration has granted approval to two CD19 CAR-T products for the treatment of R/R B-ALL, tisagenlecleucel (Tisa-cel)

J Immunother Cancer: first published as 10.1136/jitc-2023-008364 on 25 June 2024. Downloaded from http://jitc.bmj.com/ on June 26, 2024 by Exeter Team. Protected by copyright.

and brexucabtagene autoleucel (Brexa-cel), which have demonstrated high rates (70–90%) of complete remissions in both pediatric and adult R/R B-ALL.[3 4] However, long-term follow-up data reveal a significant challenge in enhancing treatment efficacy and extending survival against the emerging high relapse rate of approximately 50% within 1–2 years post-CAR-T therapy.[5 6] The underlying factors contributing to recurrence following CD19 CAR-T cell therapy are multifactorial and not fully understood to date. Most of the relapses occurring soon after CAR-T therapy were composed of $CD19^+$ relapse with poor persistence of CAR-T, while $CD19^-$ relapse were attributed to frameshift/missense CD19 mutations, alternative splicing of CD19 messenger RNA, hemizygous deletions spanning the CD19 locus and relapse related to lineage switch.[7–10] Except for CAR-T persistence and tumor antigen modulation, evidence from both independent research groups and our experiments highlights a robust association between tumor microenvironment (TME), which actively participates in tumor progression and varies with disease status, and the efficacy of CAR-T therapy.[11–13]

It has been reported that CD19 CAR-T substantially modifies the TME by boosting the number and the activity of cytotoxic effector T cells. Furthermore, CAR-T cells could specifically enhance endogenous tumor-specific T-cell response.[14] Our previous study revealed that endogenous T cells were triggered to produce more pro-inflammatory cytokines.[12] Nevertheless, the detailed phenotypic alteration and the mechanism underlying the activation of endogenous T cells may be directly influenced by CAR-T mediated antigen-dependent tumor lysis or facilitated by antigen-presenting cell (APC) assistance in reshaped TME, which have not been well elucidated.

V-domain Ig suppressor of T-cell activation (VISTA) has been identified as an inhibitory ligand that attenuates T cell-mediated immune responses, serving as the earliest immune checkpoint (IC) regulator and non-redundant compared with programmed death-ligand 1 (PD-L1) and PD-L2.[15 16] Murine tumor models demonstrated an upregulation of VISTA in TME, and VISTA monoclonal antibody (mAb) treatment impaired the suppressive character of the TME.[17] Agents targeting VISTA efficiently induced T-cell activation by converting resting and exhausted cells into functional effector cells within TME.[18] In line with the murine data, VISTA exhibits substantial upregulation in tumor-infiltrating immune cells across various cancer types and serves as a compensatory inhibitory pathway within the TME subsequent to IC antibody therapy in patients.[19 20] In addition, VISTA exhibited high expression on APC, which regulates processes of activation and repression of the immune system with not yet completely clarified mechanisms. Both T cells and myeloid cells within TME following CAR-T cell therapy are implicated with their functionalities being associated with the efficacy of CAR-T treatment. Therefore, we hypothesized that the expression pattern of VISTA on host immune cells might determine the immune activity of TME, which would be correlated with the outcome of CAR-T cell therapy.

In the present study, we observed that downregulated VISTA expression on endogenous T cells in TME following CAR-T mediated tumor lysis promoted intrinsic T-cell activation and immune function both in hematopoietic and solid tumor models. However, in interferon (IFN)-γ signaling deficient TME, high levels of VISTA persist, leading to reduced cellular activity and toxicity of endogenous T cells, and shortened mouse survival. The expression pattern of VISTA in dendritic cell (DC) was similar to that of endogenous T cells, and blockade of VISTA signaling could enhance the proliferation and function of DC-mediated homologous T cells. These findings provide valuable insights into the impact of the TME on CAR-T therapy and its association with VISTA-mediated immune response. Also, they facilitate the development and supplementation of IC inhibitors combined with CAR-T therapy.

MATERIALS AND METHODS

Mice

6–8 weeks-old male C57BL/6J and BALB/c mice weighing 18–24 g were purchased from Beijing Vital River Laboratory Animal Technology. IFN-$\gamma^{-/-}$ (B6.129S7Ifng^{tm1Ts}/J) and IFN-γR1$^{-/-}$ (B6.129S7-Ifngr1^{tm1Agt}/J) mice, kindly provided by Professor Yin (Jinan University), were bred in our animal facility under specific pathogen-free conditions at Xuzhou Medical University. C57BL/6N mice were provided by The Animal Center of Xuzhou Medical University. All experiments were approved by the Medical Ethics Committee of the Xuzhou Medical University (IACUC Issue No. 202208S094).

B-ALL mice model establishment and evaluation

The first-generation B-ALL cells were generated by infecting bone marrow cells with a retrovirus encoding P210-NGFR. Mice were examined and sacrificed in case of prostration, tousled hair, severe weakness, and paralysis of both lower limbs. B-ALL cells were identified as $CD11b^-CD19^+NGFR^+$. B-ALL cells were amplified and purified in vivo for three generations in C57BL/6J mice receiving 4.5 Gy ^{60}Co irradiations. By the third generation of B-ALL cells, the percentages of $CD11b^-CD19^+NGFR^+$ cell were 82.5%±13% and 92.1%±3.9% in spleen (SP) and bone marrow (BM), respectively. In this study, the B-ALL mice model was established by intravenous injection of $0.5–2\times10^5$ of the third-generation B-ALL cells in recipients after 4 Gy ^{60}Co irradiation.

CD19 CAR-T and hCAIX CAR-T cell generation

The CAR construct and retrovirus package were described in the previous study.[12] The CD19 CAR construct consists of the anti-murine CD19 single-chain fragment variable (scFv) domain, the transmembrane and intracellular domains of CD28, and the CD3z intracellular domain. The hCAIX CAR is composed of anti-human CAIX scFv,

J Immunother Cancer: first published as 10.1136/jitc-2023-008364 on 25 June 2024. Downloaded from http://jitc.bmj.com/ on June 26, 2024 by Exeter Team. Protected by copyright.

4-1BB co-stimulatory domain, and CD3z intracellular domain. Additionally, the retroviral vector encodes green fluorescent protein (GFP) to evaluate transduction efficiency and identify CAR-T cells. In brief, splenic $CD3^+$ T cells from male C57BL/6, IFN-$\gamma^{-/-}$ B6 and BALB/c mice were isolated and purified using EasySep negative selection reagents according to the manufacturer's instructions (STEMCELL Technologies). Purified T cells (2×10^6/mL) were activated in 24-well plate pre-coated with anti-CD3 mAb (2 µg/mL; clone17A2; BioGems), supplemented with soluble anti-CD28 mAb (2 ug/mL; clone37.51; BioGems) and hIL-2 (100 U/mL, PeproTech). Spin infections were performed 24 hours after T-cell activation using CD19 CAR or hCAIX CAR retroviral particles. Infected T cells were cultured for an additional 2 days in the presence of hIL-2 and the percentage of GFP-positive CAR-T cells was analyzed using flow cytometry.

CAR-T therapy and re-challenge experiment in B-ALL mice

B-ALL models were established in C57BL/6J, IFN-$\gamma^{-/-}$ and IFN-γR1$^{-/-}$ mice, respectively. Three days later, the mice were randomly allocated into groups and administered a single dose of either wild-type (WT) or IFN-$\gamma^{-/-}$ CD19 CAR-T cells ($0.5–1\times10^6$/mouse) via tail vein injection, while activated syngeneic T cell were given as the control group. The day of CAR-T cell administration was considered as day 0. Daily observations and recordings were conducted to monitor survival rates, body weight changes, and clinical score throughout the experiment duration. The tumor burden analysis was performed using flow cytometry. Mice with long-term survival after CD19 CAR-T therapy were re-challenged with 1×10^5 B-ALL cells per mouse. Prior to tumor cell re-challenge, the complete elimination of tumors was confirmed through-flow cytometry.

Murine lymphoma model establishment and therapy

Murine lymphoma A20 cell line, preserved in our laboratory and cultured in Roswell Park Memorial Institute (RPMI)-1640 medium supplemented with 10% fetal bovin serum (FBS), was evaluated for CD19 expression by flow cytometry. BALB/c mice were exposed to sublethal irradiation (3.5 Gy ^{60}Co) and subsequently received a subcutaneous injection of $CD19^+$A20 cells (10×10^6/mouse) into the subepidermal layer on the right underarm region, thereby establishing B-cell lymphoma models after a 4-hour interval. A20 cell seeded mice were randomly allocated to receive either activated T cell or CD19 CAR-T cell therapy after 8 days. The day of CAR-T cell administration was designated as day 0, and tumor size and body weight changes were monitored every 2 days.

Murine melanoma model establishment and therapy

The B16F10 cell line overexpressing human CAIX antigen was engineered and used to establish a subcutaneous transplantation melanoma model in C57BL/6N mice. On day 0, 100 µL of 2×10^5 B16F10 cells were injected into the subepidermal layer on the right side of the dorsal region. On day 9, marrow clearance was achieved by pretreating with 200 mg/kg cyclophosphamide. On day 10, tumor-bearing mice were randomly divided into two groups named as untreated control group and the CAR-T cell treated group (5×10^6 cells/mouse). After a period of 30 days from tumor seeding, the mice were euthanized for subsequent analysis. Tumors, draining lymph nodes (dLN), and spleens were dissected and processed into single-cell suspensions for flow cytometry analysis of endogenous T-cell quantity and functionality.

Endogenous T-cell isolation and tumor response assessment

Endogenous T cells labeled with GFP^-CD3^+ markers were isolated from splenic cells using flow cytometry from B-ALL B6 mice treated with CD19 CAR-T (trained T) or untreated (untrained T) on days 7–10. For ex vivo experiments, the purified trained and untrained endogenous T cells were co-cultured with B-ALL cells at an Effector:Target ratio of 1:1 for 24 hours. Similarly, endogenous untrained or trained T cells by CD19 CAR-T were isolated from A20 BALB/c mice, and subsequently co-cultured ex vivo with $CD19^+$ A20 or $CD19^-$A20 cells, respectively. The tumor proportions were quantified using flow cytometry. Additionally, these isolated trained and untrained T cells (4×10^5/mouse) were adoptively transferred into two groups of B-ALL mice on day 0, respectively. The proportion of B-ALL cells in peripheral blood was detected on day 16, and the survival rate of mice was recorded. The quantity, phenotype characteristics, and cytokine production of T cells in adoptively transferred mice were detected by flow cytometry.

PCR

The total genomic DNA extraction of untrained/trained endogenous T cells and CD19 CAR-T cells was performed using a DNA isolation kit (TIANGEN). Two pairs of primers were designed to amplify different sizes of CD19 scFv fragments: Forward 5'-AAGAACAAGGCCACCCTGAC-3'; Reverse 5'-GTAGTAGCCGCCGTAGATGC-3', and Forward 5'-TGAAGCTGTCCTGCAAGGTG-3'; Reverse 5'-CAGGGTGGCCTTGTTCTTGA-3'. Primers for the EGFP fragments (Forward 5'-ACGACGGCAACTACAAGACC-3'; Reverse 5'-GCCTTGATGCCGTTCTTCTG-3') were used to verify its consistency with scFv. Amplification was carried out using 2×Hot Start Taq PCR Mix (TIANGEN), with an addition of 200 ng of extracted DNA to the final volume of the PCR mixture (25 µL). Subsequently, the amplified DNA product underwent electrophoresis analysis on a gel containing agarose at a concentration of 2%, followed by visualization using the TANON MINI Space 2000 Multifunctional Gel Image Analysis System (Tanon Science & Technology).

Western blotting

For western blotting, antibodies specific to anti-VISTA, anti-STAT3, and anti-STAT3 (pY705) were purchased from Cell Signaling Technology. Antibodies specific to anti-STAT1 and anti-STAT1(pY701) were purchased

J Immunother Cancer: first published as 10.1136/jitc-2023-008364 on 25 June 2024. Downloaded from http://jitc.bmj.com/ on June 26, 2024 by Exeter Team. Protected by copyright.

from BD Bioscience. Antibodies specific to β-actin were purchased from Proteintech. All primary antibodies were used at a dilution of 1:2,000. HRP-conjugated secondary antibodies were diluted at 1:10,000 (Proteintech). B-ALL cells co-cultured with naïve T cells, activated T cells, and CAR-T cells for 6 hours, respectively, were lysed in RIPA buffer (VICMED) supplemented with Protease Inhibitor (100×; VICMED) and Phosphatase Inhibitor Cocktail (100×; Proteintech) at the indicated time points. Total lysates were cleared by spinning at 12,000 rpm for 10 min. 25 mg of lysates were subjected to SDS-PAGE and western blotting. Proteins were detected using Western ECL Substrate (UUBIO) and Tanon 5200 Chemiluminescent Imaging System (Tanon Science & Technology).

Cytotoxicity assays

B-ALL cells were co-cultured with WT or IFN-$\gamma^{-/-}$ CD19 CAR-T cells as effectors at a 1:1 ratio in 48-well plates for in vitro killing experiments. Anti-CD3 and anti-CD28 pre-stimulated T cells were used as controls. The B-ALL cell alone group was included to assess cell growth in the medium. Flow cytometry was employed to monitor the lysis of B-ALL cells after 6, 12, 24, and 48 hours.

Bone marrow-derived dendritic cell induction

BM cells were isolated from the femurs, tibias, and sciatic bone of female C57BL/6J mice aged 6– weeks. The cells were cultured in RPMI-1640 medium supplemented with 10% FBS, 1% penicillin/streptomycin, and 20 ng/mL rmGM-CSF (STEMCELL Technologies) for 3 days. On day three, all non-adherent cells were removed and fresh supplemented medium was added for an additional 3 day culture. Immature dendritic cells (DCs) were harvested on day 6. Immature DCs were stimulated with 100 ng/mL lip0polysaccharides (LPS) in a complete medium for a duration of 24 hours to induce mature DCs. Flow cytometry analysis was performed to identify bone marrow-derived dendritic cell (BMDC) as $CD11b^{+}$ $CD11c^{+}$.

T-cell proliferation and function

To detect the effect of VISTA expression of DCs on T-cell proliferation, T cells were labeled with CFSE (carboxyfluorescein diacetate, succinimidyl ester) (BioLegend) at a final concentration of 10 mM for 25 min at 4°C. Subsequently, they were pre-activated with plate-bound anti-CD3 (clone17A2; BioGems) at a concentration of 2 µg/mL for 24 hours under a condition of 37°C, 5% CO2. Following this, the T cells were co-cultured with mature or immature DCs at a ratio of 5:1 for 3 days. NSC622608 (Topscience) as a specific inhibitor of VISTA was added or not at a concentration of 5 µM to the co-culture system. The proliferation rate of T cells was assessed by measuring CFSE intensity using flow cytometry. To assess T-cell function, pre-activated T cells were co-cultured with mature or immature DCs at a ratio of 5:1 for 2 days. Brefeldin A (10 µg/mL, Invitrogen) was added to the medium during the last 6 hours of incubation to inhibit protein transport. Subsequently, flow cytometry was employed to measure T-cell cytokines including IFN-γ, tumor necrosis factor (TNF)-α, and granzyme B.

Flow cytometry and antibodies

Single-cell suspensions were obtained from the BM, spleen, and liver. Prior to flow cytometry analysis, staining was performed using the following monoclonal antibodies: CD3 FITC (fluorescein isothiocyanate) (clone17A2; BioLegend), CD3 BV650 (clone17A2; BioLegend), CD3ε PE/Cy5 (clone145-2C11; Elabscience), CD4 PE/Cyanine7 (cloneGK1.5; BioLegend), CD4 Alex Flour700 (cloneRM4-5; BioLegend); CD8a APC (allophycocyanin) (clone53-6.7; BioLegend), CD8 APC/Cyanine7 (clone53-6.7; BioLegend); CD11b PB (Pacific Blue) (cloneM1/70; BioLegend), F4/80 BV605 (cloneBM8; BioLegend), MHC-II AF700 (cloneM5/114.15.2; BioLegend), CD19 PE-cf594 (clone6D5; BioLegend), CD19 BV510 (clone6D5; BioLegend), CD11c PE-cf594 (cloneN418; BioLegend), IFN-γ PE/Cyanine7 (cloneXMG1.2; BioLegend), TNF-α APC (cloneMP6-XT22; BioLegend); Granzyme B eFlour450 (cloneM5/114.15.2; Thermo Fisher Scientific); CD62L PB (cloneMEL-1; BD Biosciences), CD44 APC/eFlour780 (cloneIM7; BD Biosciences); PD-1 PE/Cyanine7 (clone RMP1-30; BioLegend), TIGIT (Vstm3) PE (clone1G9; BioLegend); NGFR (CD271) APC (cloneME204; BioLegend), VISTA (PD-1H) PE (cloneMIH63; BioLegend), CD69 BV510 (cloneH1.2F3; BioLegend), and CD20 APC/Cyanine7 (clone SA275A11; BioLegend). For intracellular cytokine staining, cells were stimulated with PMA (50 ng/mL, Sigma) and Ionomycin (750 ng/mL, Sigma) in the presence of Brefeldin A (10 µg/mL, Invitrogen) at 37°C for 5 hours. Analyses were performed using a BD LSRFortessa Fortessa Flow Cytometer (RRID: SCR_019601), and the data was analyzed using FlowJo V.10.8.1 (BD Biosciences).

Statistical analysis

Statistical analyses and graphs were performed using GraphPad Prism V.9 software (GraphPad Prism, San Diego, RRID: SCR_002798). The data exhibited normal distribution and were presented as mean±SD or mean±SEM. Student's t-test was employed for comparing two groups with homogeneous variance, while non-parametric tests were used for unequal variance. One-way analysis of variance was conducted for multiple group comparisons. Survival rates were assessed using the log-rank test. Correlation analysis was carried out and graphs were generated using R V.4.2.1 software. After analyzing the correlation between variables across multiple data sets, trends in each data set were visualized using gglot2 (3.3.6) and ggtext (0.1). Spearman's rank correlation coefficient was used to assess the relationship between two variables. A p value of <0.05 was considered statistically significant.

J Immunother Cancer: first published as 10.1136/jitc-2023-008364 on 25 June 2024. Downloaded from http://jitc.bmj.com/ on June 26, 2024 by Exeter Team. Protected by copyright.

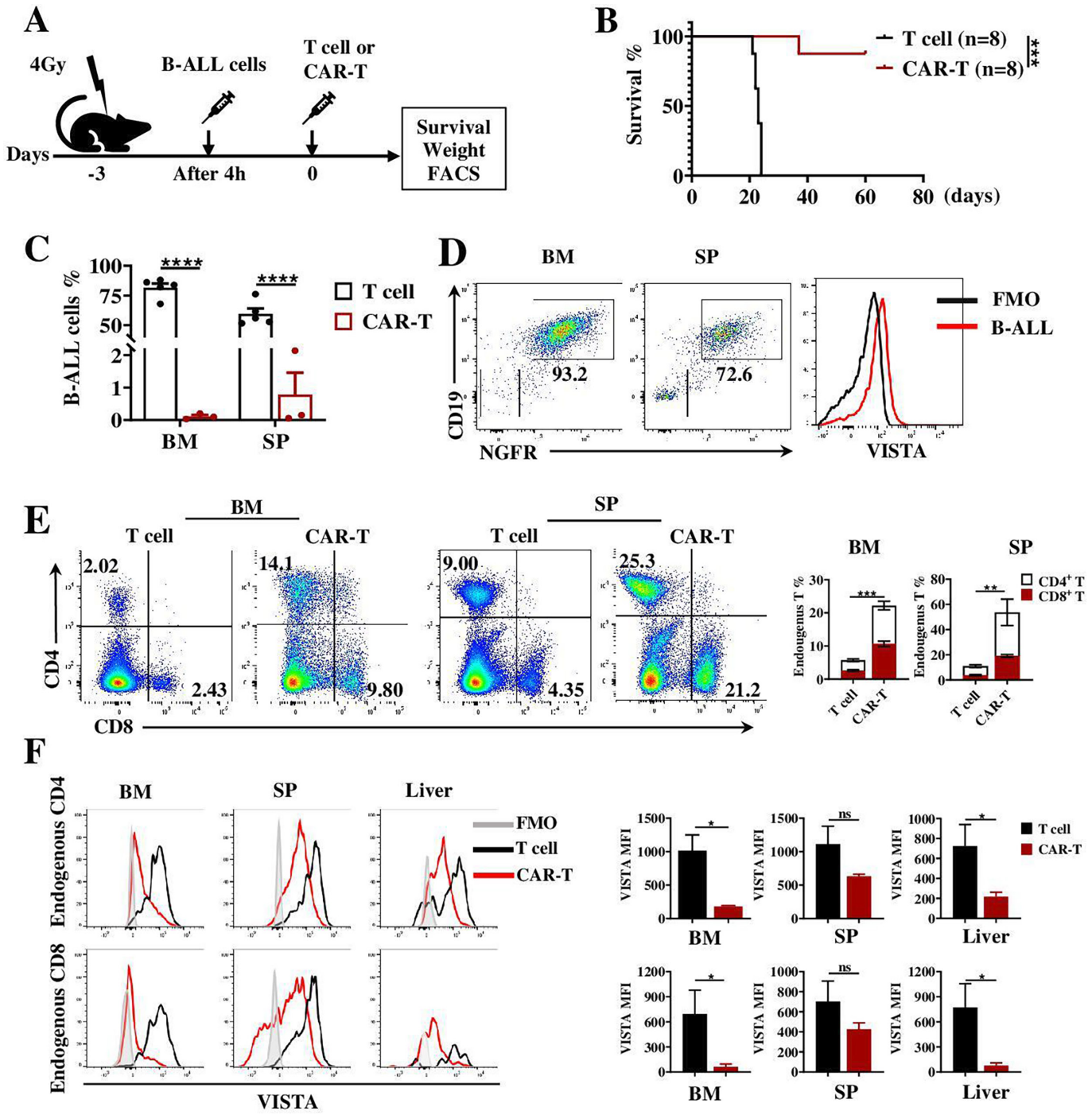

Figure 1 Decreased VISTA expression on endogenous T cells in B-ALL mice after CAR-T cell treatment. (A) The experiment design. (B) Survival of mice bearing B-ALL tumors following T cells or CAR-T cell treatment. (C) Percentages of B-ALL cells within BM and SP on day 23. Each dot represents one mouse. (D) The representative flow cytometry data showing the proportion and VISTA expression of B-ALL cells in BM and SP. (E) Percentages of endogenous $CD4^+$ T and $CD8^+$ T cells of BM and SP. (F) The fluorescence intensities of VISTA on endogenous $CD4^+$ and $CD8^+$ T cells in BM, SP and liver. The independent experiment was replicated three times. Data were mean±SD or mean±SEM, and unpaired student's t-test was used. ns, p>0.05; *p<0.05; **p<0.01; ***p<0.001; ****p<0.0001. B-ALL, B acute lymphoblastic leukemia; BM, bone marrow; CAR, chimeric antigen receptor; FMO, fluorescence minus one; SP, spleen; VISTA, V-domain Ig suppressor of T-cell activation.

RESULTS

VISTA expression was downregulated on endogenous T cells in B-ALL mice after CD19 CAR-T cell treatment

We took advantage of an immunocompetent and syngeneic model receiving C57BL/6 mice-derived BCR-ABL $P210^+$ B-ALL cells to assess CD19 CAR-T function (figure 1A). Significant longer survival was investigated in mice treated with CD19 CAR-T cells than in T cells injected control mice (figure 1B). Percentages of B-ALL cells that were labeled by CD19 and NGFR were

J Immunother Cancer: first published as 10.1136/jitc-2023-008364 on 25 June 2024. Downloaded from http://jitc.bmj.com/ on June 26, 2024 by Exeter Team. Protected by copyright.

dramatically reduced after CAR-T cell administration (figure 1C). In figure 1D VISTA level was almost undetectable gating on B-ALL, which was consistent with the previous reports that B cells were negative for VISTA expression.[15] The percentages of endogenous $CD4^+$ and $CD8^+$ T cells were consistently observed higher in CAR-T-treated mice, as anticipated (figure 1E).[12] Compared with levels of VISTA on endogenous $CD4^+$ T and $CD8^+$ T cells in CAR-T untreated mice, downregulated VISTA expression was demonstrated in BM, SP, and liver after CAR-T injection (figure 1F). These data suggested that the reduced VISTA might deactivate the immunosuppressive function of endogenous T cells to assist CAR-T cell-induced tumor clearance.

Reduction of VISTA on syngeneic T cells was not achieved solely through CAR-T cell-induced tumor lysis

It aims to clarify if the variation of VISTA is directly caused by the killing effect of CAR-T, or if it is dependent on the presence of TME. We next examined the expression of VISTA on syngeneic-activated T cells co-cultured with CAR-T and B-ALL in vitro. Flow cytometry analysis was performed as the gating strategy shown in figure 2A. The CD19 CAR-T cells were distinguished based on GFP expression, while the GFP^- cells were further segregated by CD11b expression to differentiate between myeloid and lymphocytic populations. Then the GFP^- syngeneic T cells and $NGFR^+$ B-ALL cells were identified using surface markers CD4, CD8 and CD19, respectively. The expression of VISTA was assessed in GFP^+ CAR-T cells and GFP^- syngeneic T cells (figure 2A). The death rate of B-ALL exceeded 90% after co-culturing for 6 hours, indicating that the CAR-T cells induced a potent and rapid tumor lysis compared with activated T cells (figure 2B). The results in figure 2C demonstrated that activated T cells exhibited a modest production of IFN-γ and TNF-α, which were associated with tumor cell death or senescence,[21 22] whereas significantly elevated levels were observed in the CAR-T groups. Furthermore, no difference in VISTA expression was observed between the activated T group and syngeneic GFP^- T cells in terms of tumor lysis induced by GFP^+ CAR-T cells (figure 2D). The similar pattern of VISTA expression of activated T cells in the presence or absence of tumor lysis in vitro might reflect non-optimal culture conditions that fail to mimic the complicated TME in vivo. In other words, the in vitro experiments confirmed that the VISTA expression on homologous activated T cells was not solely dependent on CAR-T cytotoxicity, but TME was essential for the remodeling of endogenous T cells.

Augmented endogenous T-cell responses within the TME following CAR-T cell therapy in solid tumor models

To ascertain the generalizability of endogenous T-cell activation within TME subsequent to CD19 CAR-T cell administration, we evaluated murine lymphoma established by subcutaneously seeded A20 cells. The administration of CD19 CAR-T cells led to a significant regression of lymphoma in mice (figure 3A). Notably, there was an increase in the number of endogenous T cells, as depicted in figure 3B. Furthermore, the activation marker CD69 exhibited higher expression on endogenous T cells within the tumor and SP, while VISTA levels were reduced and PD-1 expression showed various changes (figure 3C). Additionally, there was an elevation in tumor-killing-associated cytokines secreted by endogenous T cells (figure 3D). Furthermore, to investigate the impact of diverse CAR-T cell on endogenous T-cell function within TME, we employed hCAIX CAR-T therapy in murine $hCAIX^+$ melanoma models. Consistent findings revealed a significant increase in endogenous T-cell populations within the tumor and draining LN (figure 3E). The activation of endogenous T cells was indicated by the upregulation of CD69, while VISTA and PD-1 exhibited downregulation in both tumor and SP samples (figure 3F). IFN-γ and granzyme B production increased in tumor and dLN-derived T cells (figure 3G). In summary, the above data demonstrated that CAR-T therapy elicits the activation of endogenous T cells within the TME, regardless of the specific type of CAR-T used, encompassing both hematologic malignancies and solid tumors.

Endogenous T cell-derived IFN-γ maintains the therapeutic effect of CD19 CAR-T and regulates VISTA expression in TME

The production of IFN-γ by CAR-T cells and the responsiveness of host immune cells to IFN-γ was found to be critical for remodeling tumor immune landscape, promoting a more activated and less suppressive TME.[23] Therefore, IFN-$\gamma^{-/-}$ CAR-T cells were employed to investigate the relationship between VISTA and CAR-T efficacy in the presence or absence of IFN-γ signaling. The transfection efficiency was evaluated in both WT and IFN-$\gamma^{-/-}$ CAR-T cells, with no significant statistical difference observed (online supplemental figure 1A). In vitro lysis of B-ALL was detected in a co-cultured system involving IFN-$\gamma^{-/-}$ CAR-T or WT CAR-T cells, while tumor alone or activated T cells were used as controls, respectively. Surprisingly, IFN-$\gamma^{-/-}$ CAR-T exhibited comparable cytotoxicity to WT CAR-T cells in vitro (figure 4A). To validate the tumor clearance efficacy in vivo, we employed the same B-ALL murine models established in WT and IFN-$\gamma^{-/-}$ B6 mice for treatment with either WT or IFN-$\gamma^{-/-}$ CAR-T cells. As depicted in figure 4B, all recipient mice treated with either WT or IFN-$\gamma^{-/-}$ CAR-T survived. In comparison to untreated and T-cell control groups, there was no discernible benefit observed after administration of IFN-$\gamma^{-/-}$ CAR-T cells in IFN-$\gamma^{-/-}$ mice. Body weight change and clinical score confirmed that there were no differences between mice treated with WT or IFN-$\gamma^{-/-}$ CAR-T cells. However, IFN-$\gamma^{-/-}$ recipients displayed lower body weight and higher clinical score (figure 4C–D). These findings suggest that the efficacy of CAR-T cells is not solely reliant on their production of IFN-γ, and it is

J Immunother Cancer: first published as 10.1136/jitc-2023-008364 on 25 June 2024. Downloaded from http://jitc.bmj.com/ on June 26, 2024 by Exeter Team. Protected by copyright.

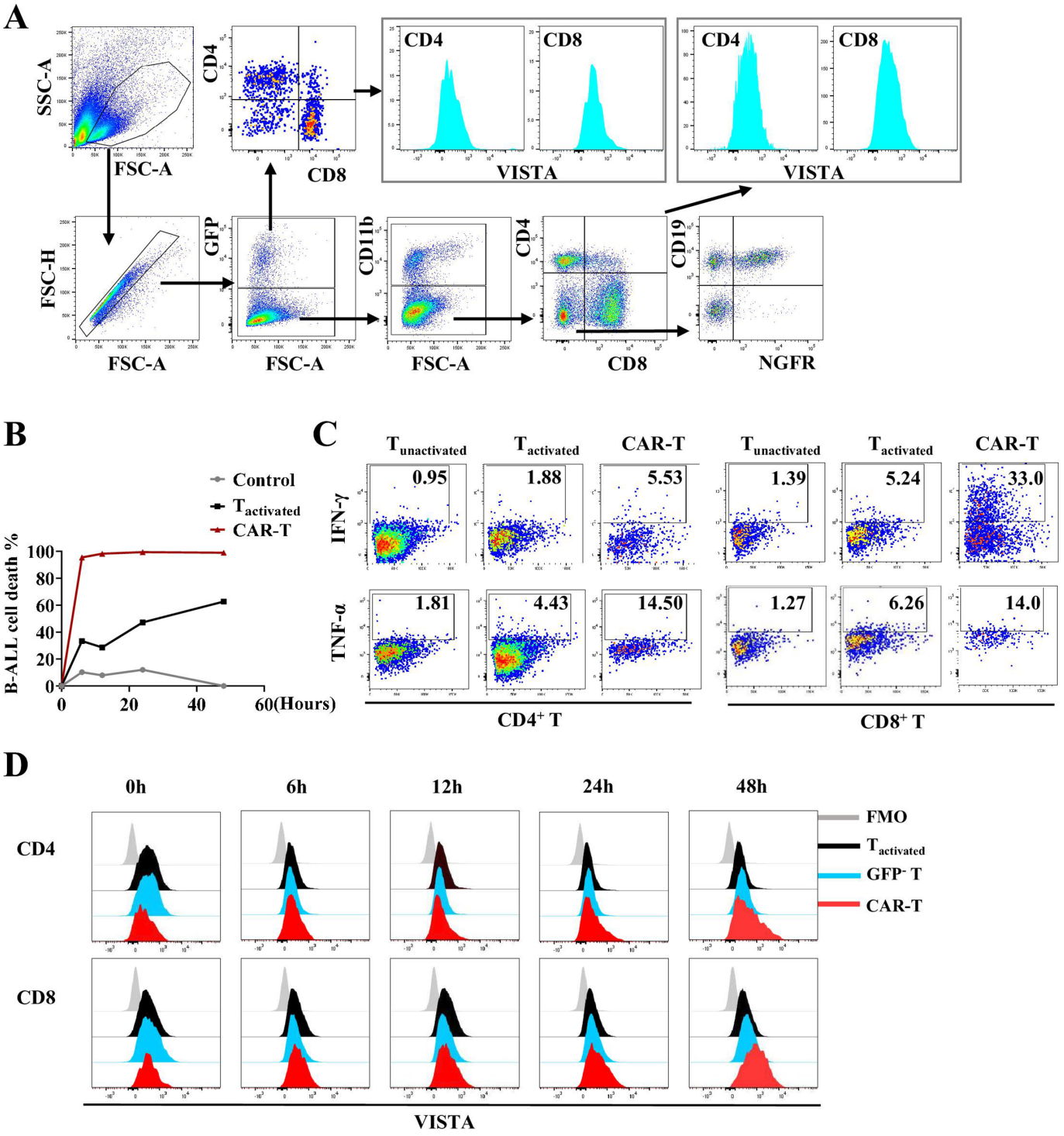

Figure 2 CAR-T cell-induced tumor lysis was not sufficient to reduce VISTA expression on syngeneic activated T cell. (A) Gating strategy of flow cytometry. (B) Percentages of B-ALL cell death in vitro. B-ALL cell alone or co-cultured with purified T-cell stimulated with anti-CD3 and anti-CD28 ($T_{activated}$) in vitro were used as the control and T-cell groups, respectively. (C) The production of cytokines was evaluated in the co-culture cellular system for 6 hours. Naïve T cells were included as a control group without antibody activation ($T_{unactivated}$). (D) The representative flow cytometry histograms of VISTA levels. The T cells lacking CAR chimerism in the CAR-T groups were designated as GFP^- T cells. Three independent experiments were repeated. B-ALL, B acute lymphoblastic leukemia; CAR, chimeric antigen receptor; FMO, fluorescence minus one; GFP, green fluorescent protein; VISTA, V-domain Ig suppressor of T-cell activation.

plausible that IFN-γ secreted by cells within the TME may serve as a compensatory factor. Consequently, we investigated endogenous T cells as a crucial cellular source of IFN-γ. The results demonstrated that T cells in the WT CAR-T mice exhibited the highest level of IFN-γ production. Although the IFN-γ levels were

J Immunother Cancer: first published as 10.1136/jitc-2023-008364 on 25 June 2024. Downloaded from http://jitc.bmj.com/ on June 26, 2024 by Exeter Team. Protected by copyright.

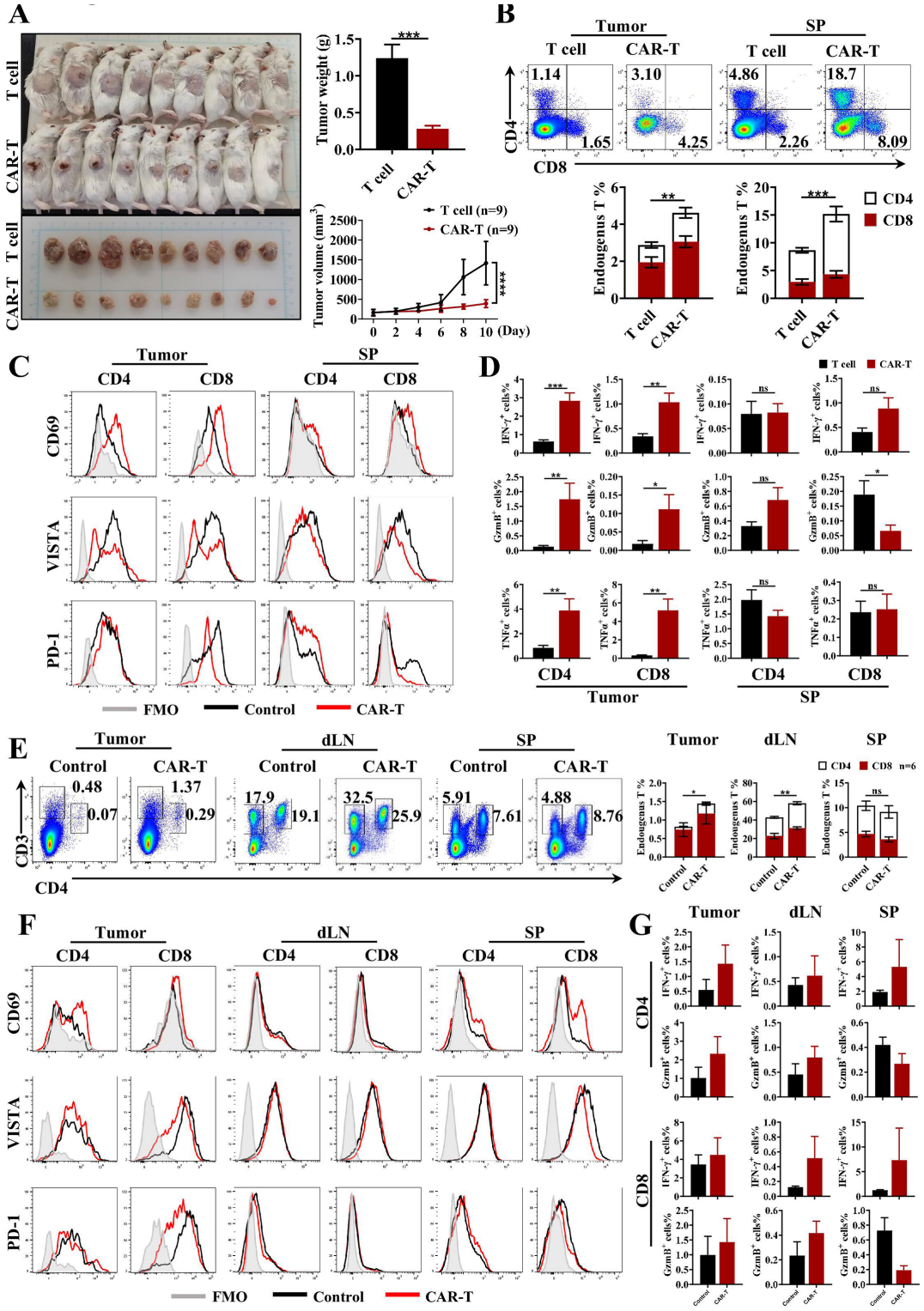

Figure 3 Enhanced endogenous T-cell responses within the tumor microenvironment following CAR-T cell therapy in solid tumor models. The A20 lymphoma mice were subcutaneously inoculated on –8 days and subsequently treated with or without CD19 CAR-T cells as day 0 (n=9). (A) Tumor size, weight and volume in CAR-T treated and untreated lymphoma mice. (B) The percentages of endogenous T-cell infiltrated in tumor tissue and spleen on day 11. (C) The representative flow cytometry histograms of CD69, VISTA, and PD-1 of endogenous T cells from lymphoma mice. (D) Cytokine production of endogenous T cells in tumor and spleen of lymphoma mice with or without CD19 CAR-T cell therapy. (E–G) exhibited the data from hCAIX CAR-T treated and untreated melanoma murine model for 30 days (n=6). (E) The percentages of endogenous T cells infiltrated in the tumor, in the draining LN and spleen were evaluated, respectively. (F) Expression of CD69, VISTA, and PD-1 were detected in endogenous T cells. (G) The secretion of cytokines in endogenous T cells from tumor tissue, draining LN and spleen were exhibited. ns, p>0.05; *p<0.05; **p<0.01; ***p<0.001. CAR, chimeric antigen receptor; dLN, draining lymph nodes; FMO, fluorescence minus one; PD-1, programmed cell death protein-1; SP, spleen; VISTA, V-domain Ig suppressor of T-cell activation.

J Immunother Cancer: first published as 10.1136/jitc-2023-008364 on 25 June 2024. Downloaded from http://jitc.bmj.com/ on June 26, 2024 by Exeter Team. Protected by copyright.

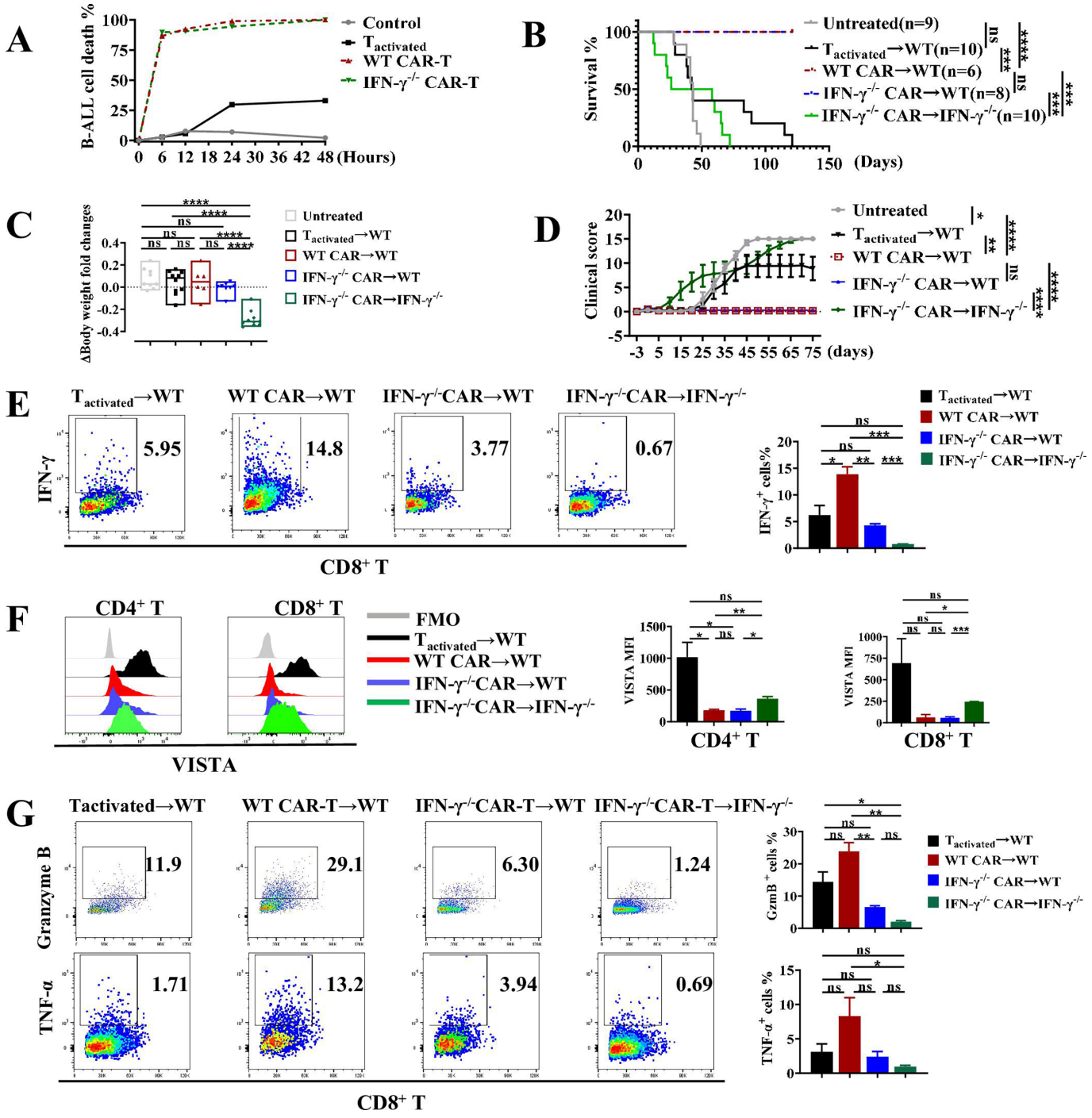

Figure 4 The production of IFN-γ within tumor microenvironment exerts an influence on the VISTA expression and functionality of endogenous T cells. (A) Evaluation of the killing effect of WT and IFN-$\gamma^{-/-}$ CAR-T cells in vitro. Two independent experiments were repeated. (B–D). The survival rate, body weight changes and clinical score were recorded in recipients treated with WT or IFN-$\gamma^{-/-}$ CAR-T cells. (E) The representative flow cytometry of IFN-γ production and statistical analysis of endogenous $CD8^+$ T cells in BM. (F) The fluorescence intensities of VISTA on endogenous $CD4^+$ and $CD8^+$ T cells of BM. (G) The representative flow cytometry plots and statistical analysis showed secretion of TNF-α and granzyme B from $CD8^+$ T cells. The independent in vivo experiment was repeated twice. Data were mean±SD or mean±SEM, and one-way analysis of variance was used to do statistical analysis. ns, p>0.05; *p<0.05; **p<0.01; ***p<0.001; ****p<0.0001. BM, bone marrow; CAR, chimeric antigen receptor; IFN, interferon; TNF, tumor necrosis factor; VISTA, V-domain Ig suppressor of T-cell activation; WT, wild-type.

comparatively lower in the IFN-$\gamma^{-/-}$ CAR-T group compared with the WT group, they still remained significantly higher than those observed in the IFN-$\gamma^{-/-}$ recipient group (figure 4E). The VISTA fluorescence intensity on endogenous $CD4^+$ and $CD8^+$ T cells was found to be increased in IFN-$\gamma^{-/-}$ recipients, but not in WT mice following IFN-$\gamma^{-/-}$ CAR-T treatment (figure 4F). In line with these findings,

J Immunother Cancer: first published as 10.1136/jitc-2023-008364 on 25 June 2024. Downloaded from http://jitc.bmj.com/ on June 26, 2024 by Exeter Team. Protected by copyright.

the downstream proteins pSTAT1 and pSTAT3 of IFN-γ signaling exhibited a gradual increase in naïve T cells, activated T cells, and CAR-T cells, concomitant with a decrease in VISTA expression; however, no significant changes were observed in total STAT1 and STAT3 levels (online supplemental figure 1B). Additionally, lower levels of granzyme B and TNF-α were observed in both WT and IFN-$\gamma^{-/-}$ recipients injected with IFN-$\gamma^{-/-}$ CAR-T cells (figure 4G). The above data suggests that the regulation of IFN-γ on the TME may exert a significant influence on the expression of VISTA and the functionality of endogenous T cells, thereby highlighting their dual role as both compensatory sources of IFN-γ for CAR-T cells and valuable allies in tumor clearance.

Characteristics of endogenous T cells within TME following CAR-T therapy

To elucidate the value of endogenous T cells trained by CD19 CAR-T, we assessed the cytotoxicity of isolated $GFP^{-}CD3^{+}$ T cells through ex vivo co-culture with B-ALL and adoptive transfer to B-ALL mice, respectively. The tumor-clearing capacity of CD19 CAR-T-trained endogenous T cells was more pronounced compared with untrained T cells, as evidenced by both the co-culture system (figure 5A) and adoptive transfer experiments (figure 5B). To exclude the potential contamination of CAR-T cell-induced tumor lysis, we evaluated the purification of endogenous T cells and amplified fragments of CD19 scFv; however, no amplification of scFv was observed in trained endogenous T cells (online supplemental figure 2A,B). Furthermore, ex vivo co-cultures were performed using untrained and trained endogenous T cells derived from CD19 CAR-T treated A20 mice with $CD19^{+}$ A20 or $CD19^{-}$ A20 cells, respectively. Consistent with findings in B-ALL B6 mice, trained T cells demonstrated tumor cytotoxicity, whereas CD19 CAR-T exhibited no impact on $CD19^{-}$ A20 cells (online supplemental figure 2C,D). Importantly, CD19 CAR-T trained endogenous T cells injected into B-ALL mice confer significant benefits (figure 5C). Moreover, significantly higher levels of CD69 were observed in the BM and SP of B-ALL mice that received trained endogenous T cells, while lower levels of VISTA and PD-1 were detected (figure 5D). These findings indicate the enhanced tumor reactivity of endogenous T cells following CD19 CAR-T therapy, characterized by heightened expression of active markers and increased cytokine production (online supplemental figure 3A). Furthermore, based on the surface markers CD44 and CD62L, endogenous T cells exhibited three distinct subsets: effector cells ($CD44^{+}CD62L^{-}$), memory cells ($CD44^{+}CD62L^{+}$), and naïve-like cells ($CD44^{-}CD62L^{+}$) in online supplemental figure 3B and figure 5E. Effector cells of $CD4^{+}$ T predominated with no observed differences among the groups in the BM. Within the spleen, reduction in IFN-γ levels from CAR-T cells resulted in decreased percentages of effector and memory T cells, while an increase was observed in the naïve-like $CD4^{+}$ T cell (figure 5E). In mice treated with IFN-$\gamma^{-/-}$ CAR-T, a decrease of $CD8^{+}$ memory T subset in BM was evident, and this reduction was more pronounced within the TME completely lacking IFN-γ signaling. Additionally, in IFN-$\gamma^{-/-}$ recipients there was a decrease in splenic effector $CD8^{+}$ T cell accompanied by an increased proportion of naïve-like T subsets (figure 5E). Endogenous T cells were further investigated on B-ALL re-challenge in WT and IFN-$\gamma^{-/-}$ recipients following CAR-T treatment. The experimental design was depicted in online supplemental figure 4A. In CAR-T treated mice, longer survival, alleviated clinical manifestations and delayed disease occurrence were observed compared with the newly established B-ALL model (figure 5F). However, no difference was presented in CAR-T proportion among groups (online supplemental figure 4B). A higher proportion of memory and quiescent naïve-like endogenous $CD4^{+}$ T cells were found in the BM of CAR-T treated mice with long-term remission, while most endogenous $CD8^{+}$ T cells exhibited memory phenotypes. On tumor re-challenge, elevated levels of effector $CD4^{+}$ and $CD8^{+}$ T cells with higher cytokine secretion were induced in both wild-type and IFN-$\gamma^{-/-}$ recipients, independent of IFN-γ production by CAR-T (figure 5G and online supplemental figure 4C). The VISTA expression level was highest in memory $CD4^{+}$ T cells and successively decreased in naïve-like and effector $CD4^{+}$ T cells, while no significant difference was observed among $CD8^{+}$ T-cell subsets (figure 5H). Figure 5I depicted the comprehensive profiles of endogenous T cells across groups, illustrating a close association between VISTA expression patterns and the composition and immune activity of T-cell subpopulations.

The subpopulations of VISTA and PD-1 exhibit independent and distinct expression patterns

The IC molecular detection results revealed that PD-1 and T cell immunoreceptor with Ig and ITIM domains (TIGIT) were highly expressed on cells of IFN-$\gamma^{-/-}$ recipients with the shortest survival, whereas their expression levels were low on endogenous T cells of WT recipients after remission (figure 6A–B). In conjunction with the diverse VISTA expression patterns depicted in figure 4A, these findings suggest a diminished inhibitory function of ICs on endogenous T cells during the early remissive stage of CAR-T therapy. Whereas, in the absence of IFN-γ within the TME, endogenous T cells exhibit an immunosuppressive state regulated by ICs. Furthermore, prolonged remissive mice from WT CAR-T treated host showed low PD-1 expression and high VISTA expression on endogenous T cells, suggesting a resting state of them (figure 6C–D). However, the expression of PD-1 on endogenous T cells in CAR-T treated hosts was once

J Immunother Cancer: first published as 10.1136/jitc-2023-008364 on 25 June 2024. Downloaded from http://jitc.bmj.com/ on June 26, 2024 by Exeter Team. Protected by copyright.

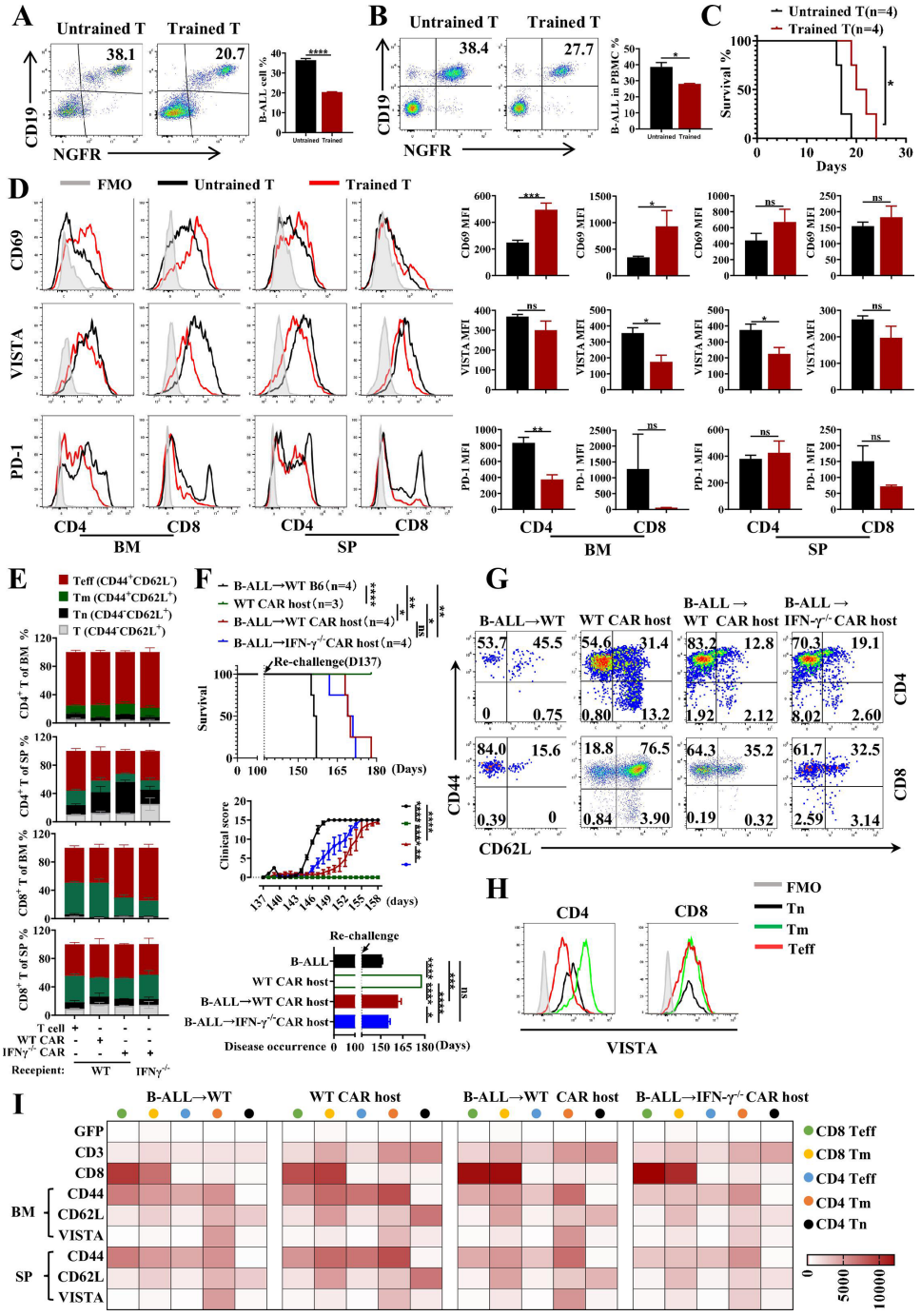

Figure 5 Tumor reactivity and phenotype characteristics of endogenous T cells. Endogenous T cells named as trained and untrained T cells, respectively, were isolated from CD19 CAR-T treated and untreated B-ALL mice on days 7–10. (A) Isolated endogenous T cells were co-cultured with B-ALL ex vivo for 24 hours and the percentages of B-ALL were detected. (B) Isolated trained and untrained T cells were adoptive transferred to B-ALL mice on day 0, and the burden of B-ALL in PBMC were detected on day 16. (C) The survival rate of B-ALL mice following adoptive transferred trained and untrained endogenous T cells. (D) The representative histograms and statistical analysis of MFI of surface markers CD69, VISTA, and PD-1 on T cells from endogenous T-cell adoptive transferred mice. (E). The compositions of the endogenous $CD4^+$ and $CD8^+$ T subsets in WT and IFN-$\gamma^{-/-}$ recipients receiving WT or IFN-$\gamma^{-/-}$ CAR-T cells, respectively. (F) Survival rate, the clinical score and disease occurrence of B-ALL cell re-challenged CAR-T Treated host were recorded. Hosts treated with CAR-T cells without re-challenge sustained remission and observation was concluded on day 42. (G) Representative flow cytometry plots showed the endogenous $CD4^+$ and $CD8^+$ T cells subsets in mice following re-challenge. (H) The levels of VISTA on endogenous $CD4^+$ and $CD8^+$ T subsets. (I) Heatmap analysis of the phenotypic characteristics of endogenous $CD4^+$ and $CD8^+$ T cells in mice following re-challenge. ns, p>0.05; *p<0.05; **p<0.01; ***p<0.001; ****p<0.0001. B-ALL, B acute lymphoblastic leukemia; BM, bone marrow; CAR, chimeric antigen receptor; FMO, fluorescence minus one; IFN, interferon; MFI, median fluorescence intensity; PBMC, peripheral blood mononuclear cell; cell; PD-1, programmed cell death protein-1; SP, spleen; VISTA, V-domain Ig suppressor of T-cell activation; WT, wild-type; .

J Immunother Cancer: first published as 10.1136/jitc-2023-008364 on 25 June 2024. Downloaded from http://jitc.bmj.com/ on June 26, 2024 by Exeter Team. Protected by copyright.

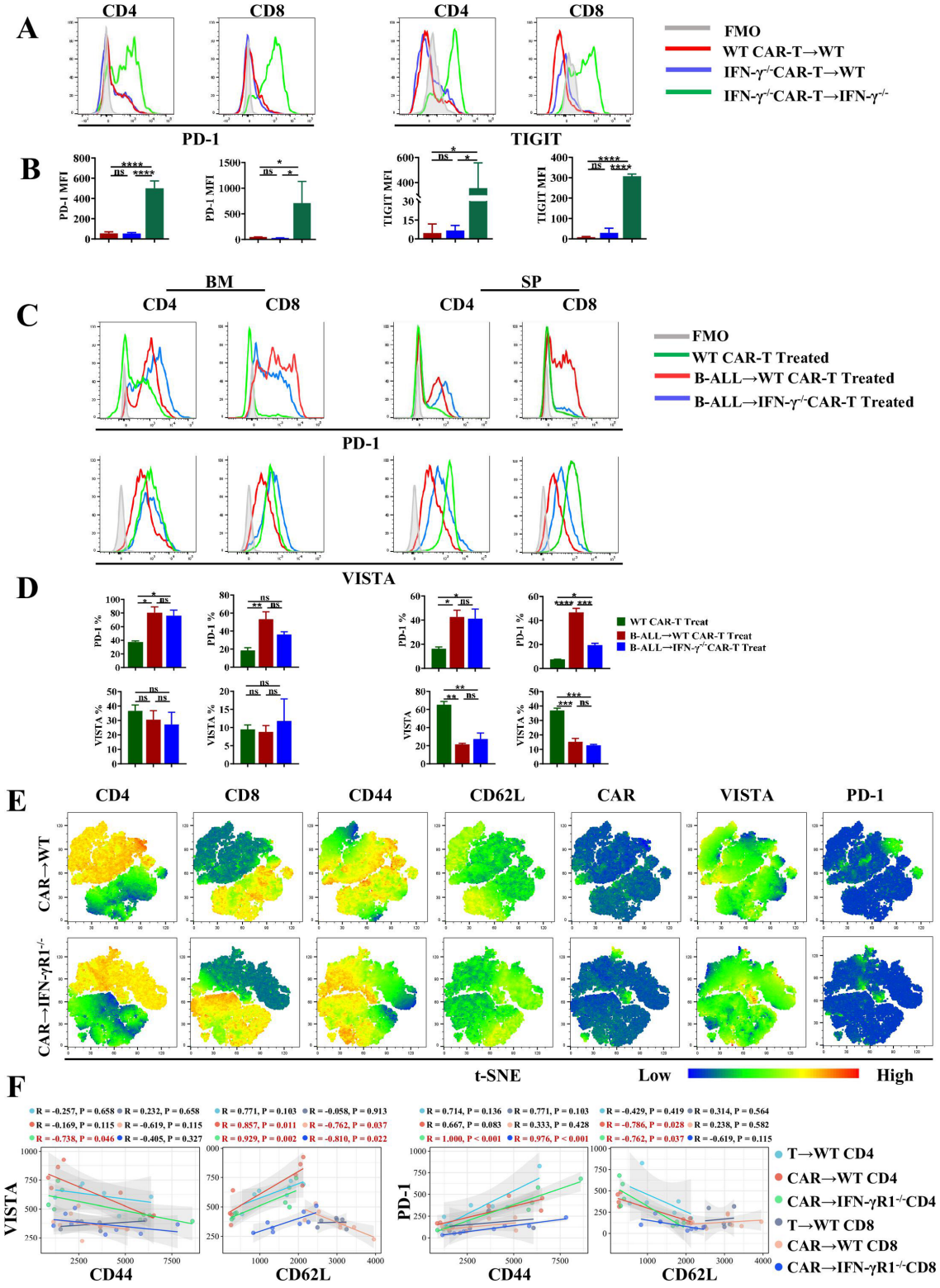

Figure 6 The expression of VISTA and PD-1 are independent on distinct T-cell subsets. (A–B). The MFI and statistical analysis of PD-1 and TIGIT expression of endogenous CD4$^+$ and CD8$^+$ T cells in BM of recipients treated with WT or IFN-$\gamma^{-/-}$ CAR-T cells. (C–D) In B-ALL re-challenge experiment, the MFI and statistical analysis of PD-1 and VISTA expression of endogenous CD4$^+$ and CD8$^+$ T cells in BM and SP. (E) WT and IFN-γR1$^{-/-}$ recipients were used to establish the B-ALL model following CAR-T therapy. VISTA and PD-1 distribution on endogenous T subsets were analyzed by t-SNE panoramic expression heat map. (F) Analysis of the correlation of VISTA and PD intensity with CD44 and CD62L levels, respectively. ns, p>0.05; *p<0.05; **p<0.01; ***p<0.001; ****p<0.0001. B-ALL, B acute lymphoblastic leukemia; BM, bone marrow; CAR, chimeric antigen receptor; FMO, fluorescence minus one; IFN, interferon; MFI, median fluorescence intensity; PD-1, programmed cell death protein-1; SP, spleen; t-SNE, t-distributed stochastic neibor embedding; TIGIT, T cell immunoreceptor with Ig and ITIM domains; VISTA, V-domain Ig suppressor of T-cell activation; WT, wild-type.

J Immunother Cancer: first published as 10.1136/jitc-2023-008364 on 25 June 2024. Downloaded from http://jitc.bmj.com/ on June 26, 2024 by Exeter Team. Protected by copyright.

again induced to be upregulated on re-exposure to B-ALL, while the level of VISTA exhibited varying degrees of decrease across all groups. Compared with the IFN-$\gamma^{-/-}$ CAR-T group, the reduction of VISTA on T cells in the WT CAR-T group was more pronounced, indicating a stronger immune activity of endogenous T cells (figure 6C–D). Then, analysis of T-cell populations using t-distributed stochastic neibor embedding (t-SNE) in IFN-γR1$^{-/-}$ recipients confirmed that VISTA and PD-1 were distributed among distinct subpopulations of T cells (figure 6E). Subpopulation localization analysis revealed a negative correlation between VISTA and CD44 expression, as well as a positive correlation between VISTA and CD62L expression. Conversely, PD-1 showed a positive correlation with CD44 expression and a negative correlation with CD44 expression (figure 6F).

Downregulated VISTA expressed on DC after CAR-T treatment but increased in IFN-γ depleted TME

The CAR-T cell therapy modulates the functionality of myeloid cells within the TME to enhance endogenous T-cell immunity and facilitate efficient tumor eradication, potentially through its impact on VISTA expression in CD11b positive myeloid cells.[19 24] Our in vitro data revealed a slight decrease in VISTA expression within CD11b^{+} myeloid cells, including CD11c^{+} DCs and F4/80^{+} macrophages, on exposure to B-ALL; however, no significant difference was observed with or without CAR-T cell-mediated tumor killing (online supplemental figure 5A,B). Interestingly, a significant reduction in VISTA expression was observed in total myeloid cells and DCs in the BM, SP, and liver of CAR-T-treated mice. Macrophages exhibited an obvious decrease in VISTA levels in the liver, along with downregulated trends in BM and SP (figure 7A). Furthermore, we observed an upregulation of VISTA on DCs in mice with complete deletion of the IFN-γ signal (figure 7B). Similar data from IFN-γR1$^{-/-}$ recipients confirmed elevated VISTA expression on DCs when there was a deficiency of IFN-γ signaling within the TME (figure 7C). The expression of major histocompatibility complex II on DCs from IFN-γR1$^{-/-}$ recipients was found to be reduced compared with WT recipients, indicating a decrease in immune activity that is associated with elevated VISTA expression (figure 7D). The above data demonstrates the dependence of the VISTA variety of DCs on the TME, as well as the involvement of CAR-T-induced host immune response.

Inhibition of VISTA signaling enhanced DC-mediated syngeneic T-cell proliferation and function

To evaluate the impact of DCs on T-cell response subsequent to VISTA signaling inhibition, we conducted a CFSE-based proliferation assay to examine the proliferative capacity of T cells on in vitro stimulation with anti-CD3 and anti-CD28. BM-derived DCs were identified and stimulated in vitro using LPS to induce maturation (online supplemental figure 6). VISTA-specific inhibitor NSC622608 was employed to block the VISTA signal. The inclusion of immature or mature DCs in the co-culture system with T cells significantly enhanced T-cell proliferation (figure 8A). Remarkably, the presence of NSC622608 in the co-culture system with DCs resulted in substantial increases in T-cell proliferation and division; however, minimal effects were observed on activated T cells without DCs (figure 8A–B). Consistent with T-cell expansion, mature DCs treated with a VISTA inhibitor exhibited higher levels of IFN-γ and granzyme B secretion by CD4^{+} and CD8^{+} T cells (figure 8C). These findings highlight the pivotal role played by VISTA in the suppressive effects exerted by DCs on T-cell responses. Furthermore, these data indicate the existence of a regulatory loop involving IFN-γ-induced VISTA expression on syngeneic T cells and DCs.

DISCUSSION

Recently, emerging evidence has demonstrated that the antitumor activity mediated by CAR-T cells is predominantly dependent on cellular cross-talk within the TME, encompassing both solid and hematologic malignancies.[14 25] The TME consists of diverse cell populations and acellular components that collectively contribute to the intricate interplay of pro-immune and immunosuppressive signaling pathways. Endogenous T cells were activated within TME following CAR-T cell treatment, and T-cell gene signature was enriched in patients who achieved durable responses.[26 27] Co-expression of endogenous T-cell receptor plus CAR led to superior persistence of T cells and significantly prolonged leukemia control in vivo.[28] However, the regulation of endogenous T-cell activation, phenotypic characteristics, and expansion remain poorly explored. Herein, we demonstrate that CAR-T cell treatment effectively abrogates VISTA mediate immunosuppression of endogenous T cells in comparison to that in the absence of CAR-T, which is tightly regulated by IFN-γ signaling within TME.

CAR-T therapy has the potential to shape the TME, creating a context permissible for eliciting endogenous antitumor immunity. It is favorable or detrimental with respect to benefiting from CAR-T treatment. Compared with untreated conditions, CAR-T treatment resulted in a notable reduction of VISTA expression on endogenous T cells, potentially disrupting their self-quiescence and promoting conversion to an activated state.[16] This observation may provide one explanation for the activation of endogenous T cells within TME. Conversely, treatment with VISTA monoclonal antibody increased the peripheral population of tumor-specific T cells and enhanced the infiltration, proliferation, and effector molecules such as IFN-γ and granzyme B of tumor-reactive T cells within the TME.[17] In this study, we observed that deficiency of IFN-γ within TME upregulated VISTA expression on endogenous T cells and attenuated their cytotoxicity by reducing TNF-α and granzyme B production. These findings suggest the existence of a potential feedback loop

J Immunother Cancer: first published as 10.1136/jitc-2023-008364 on 25 June 2024. Downloaded from http://jitc.bmj.com/ on June 26, 2024 by Exeter Team. Protected by copyright.

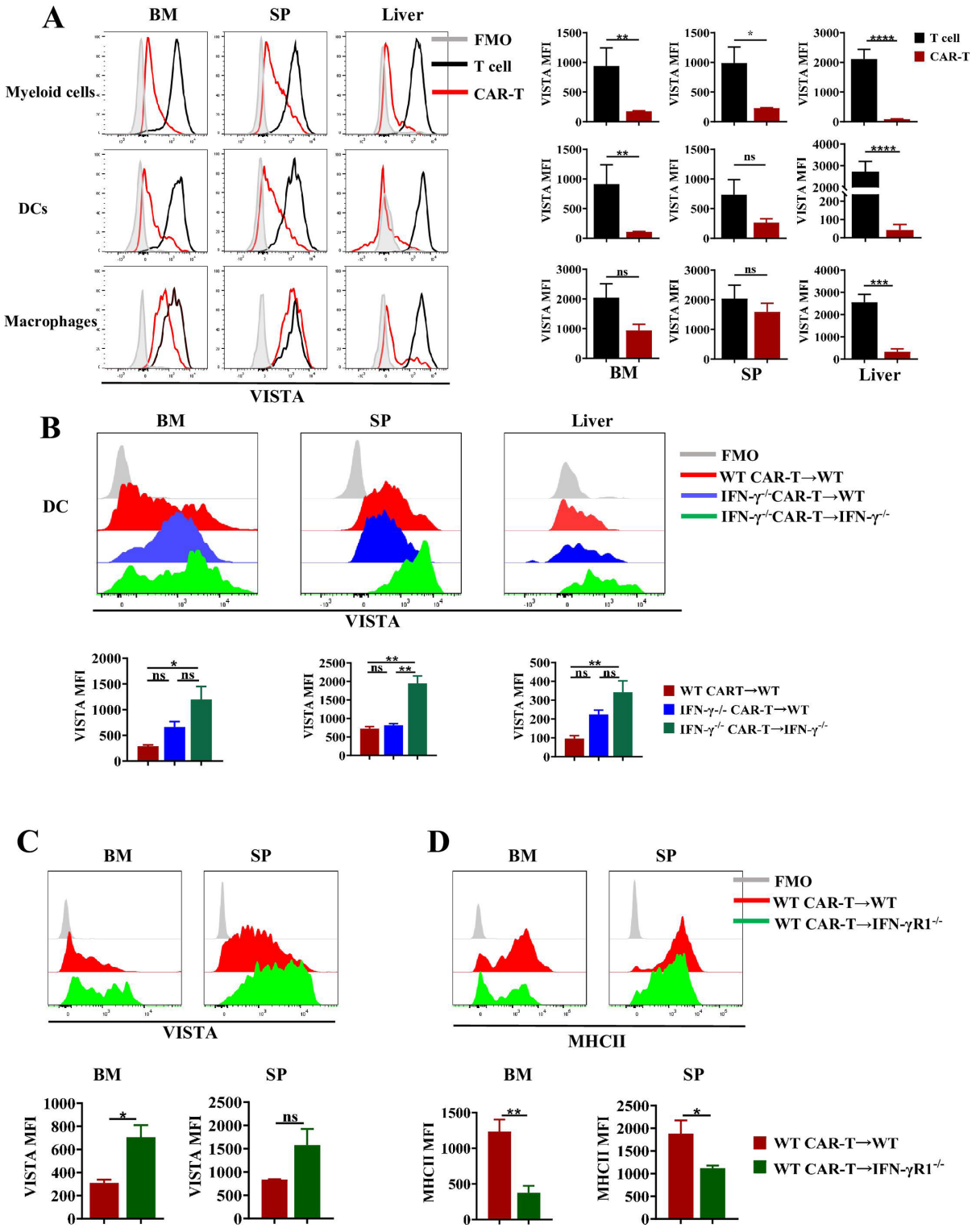

Figure 7 VISTA expression on myeloid cell subsets dependent on CAR-T induced tumor microenvironment. (A) The MFI and statistical analysis of VISTA expression on total CD11b^{+} myeloid cells, DCs and macrophages within BM, SP and liver in B-ALL mice with or without CAR-T therapy. (B) The variety of VISTA levels on DCs in WT and IFN-$\gamma^{-/-}$ recipients following CAR-T administration. (C) The MFI and statistical analysis of VISTA expression on DCs of B-ALL seeded WT and IFN-γR1$^{-/-}$ recipients following CAR-T therapy. (D) The levels of MHC-II on DCs from CAR-T-treated WT and IFN-γR1$^{-/-}$ recipients were detected by flow cytometry. ns, p>0.05; *p<0.05; **p<0.01; ***p<0.001; ****p<0.0001. B-ALL, B acute lymphoblastic leukemia; BM, bone marrow; CAR, chimeric antigen receptor; DC, dendritic cell; FMO, fluorescence minus one; IFN, interferon; MFI, median fluorescence intensity; MHC, major histocompatibility complex; VISTA, V-domain Ig suppressor of T-cell activation; WT, wild-type.

J Immunother Cancer: first published as 10.1136/jitc-2023-008364 on 25 June 2024. Downloaded from http://jitc.bmj.com/ on June 26, 2024 by Exeter Team. Protected by copyright.

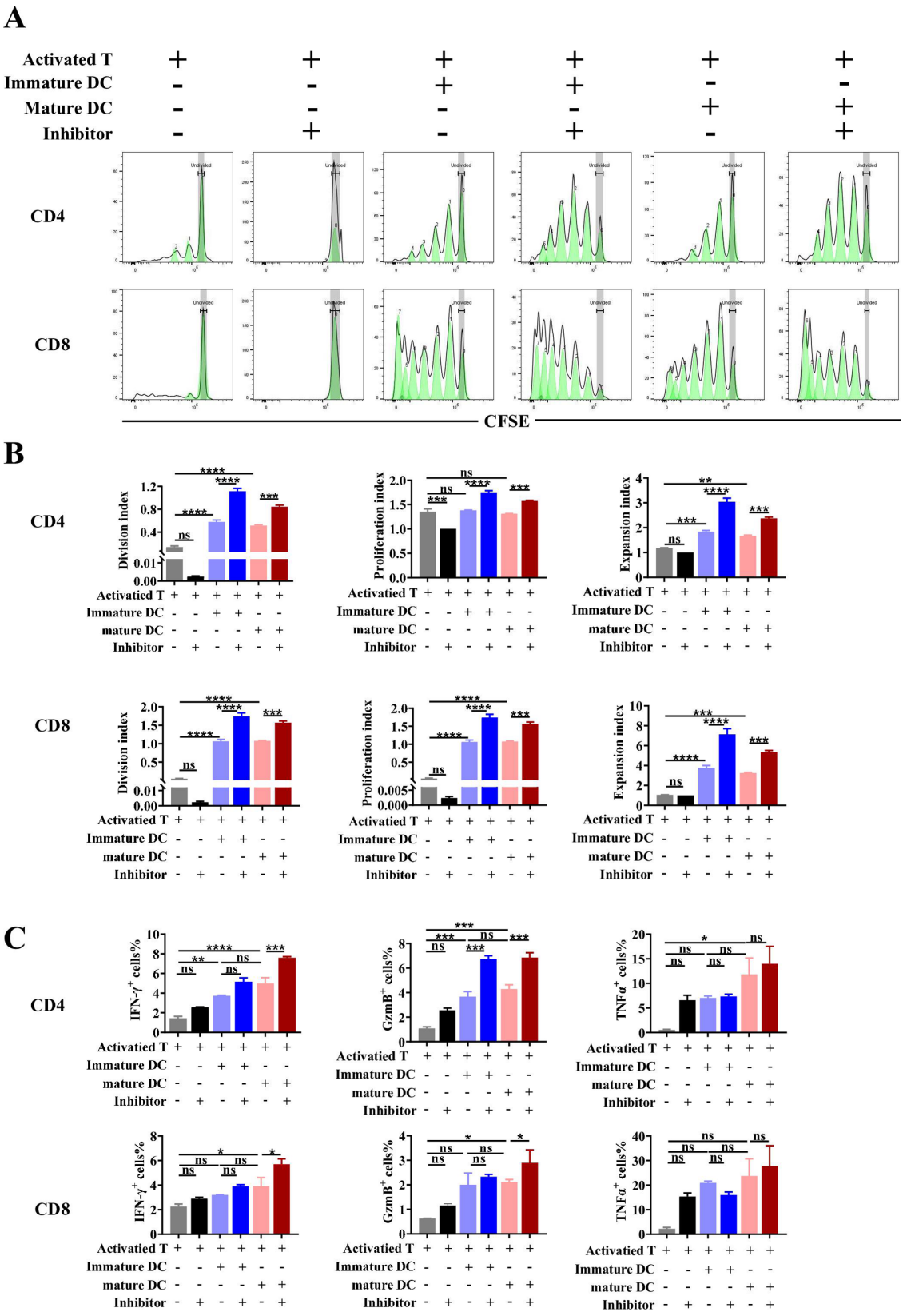

Figure 8 VISTA inhibitor promote DC induced T-cell proliferation and cytokine production. Co-culturing of bone marrow-derived dendritic cells and activated T cells for 48 hours or 72 hours in the presence or absence of VISTA inhibitor NSC622608. (A) The representative flow cytometry histograms of CFSE-labeled $CD4^+$T and $CD8^+$T cell. (B) Statistics analysis showed the $CD4^+$T and $CD8^+$ T-cell proliferation, division and expansion. (C) The percentages of IFN-γ, granzyme B and TNF-α producing $CD4^+$T and $CD8^+$ T cells were calculated. The independent experiment was repeated twice. ns, p>0.05; *p<0.05; **p<0.01; ***p<0.001; ****p<0.0001. CFSE, carboxyfluorescein diacetate, succinimidyl ester; DC, dendritic cell; IFN, interferon; TNF, tumor necrosis factor; VISTA, V-domain Ig suppressor of T-cell activation.

J Immunother Cancer: first published as 10.1136/jitc-2023-008364 on 25 June 2024. Downloaded from http://jitc.bmj.com/ on June 26, 2024 by Exeter Team. Protected by copyright.

involving IFN-γ, VISTA, and T-cell function. Although our study did not detect direct regulation of VISTA levels by IFN-γ, data from the IFN-γR1$^{-/-}$ recipient model and in vitro cell co-culture system confirmed that IFN-γ signaling negatively regulates VISTA expression on T cells.

VISTA is expressed on both T cells and APCs. VISTA on T cells directly transmits inhibitory signals to suppress T-cell activation in a T cell-intrinsic manner. Additionally, it may act as a ligand on APCs to exert extrinsic mechanisms for suppressing T-cell activity.[29 30] The downregulation of VISTA on DCs, which exhibited a similar expression pattern to endogenous T cells, was investigated in CAR-T-treated mice with demonstrated efficacy, suggesting a positive correlation between their functionality linked by VISTA. It has been reported that VISTA expressed on BMDCs can suppress antigen-specific T-cell activation during cognate interactions between them.[15] Our in vitro experiments showed that inhibition of VISTA promotes DC-induced cognate T-cell proliferation and cytotoxicity-related cytokine production. Consistent with reports indicating that blockade of VISTA diminishes the T cell-suppressive functions of tumor-associated DCs, leading to a stimulatory TME that promoted T-cell infiltration and activation.[31] Therefore, the above data demonstrated that VISTA is a critical IC protein capable of simultaneously reprogramming endogenous T cells and myeloid cells within TME following CAR-T treatment.

The inhibitory ICs within the TME have been implicated in facilitating immune evasion of tumor cells. Currently, drugs targeting PD-1/PD-L1 pathway have gained approval for clinical use in patients. However, the clinically validated effective response rate of targeting PD-1/PD-L1 is only 20–40%.[32] This limited efficacy can be attributed primarily to the emergence of resistance mechanisms mediated by additional ICs. VISTA is constitutively expressed on naïve T cells and plays a critical role in enforcing quiescence.[16] Following T-cell activation, cytotoxic T-lymphocyte associated protein 4 (CTLA-4) transiently appears on the cell surface and restricts co-stimulation to inhibit T-cell activation during the priming stage. PD-1 is expressed later during priming and inhibits T cells at the effector stage. Therefore, an interesting hypothesis arises that targeting VISTA prior to or in combination with PD-1 or CTLA-4 blockade could enhance T-cell response by overcoming limitations associated with priming and subsequent exhaustion. Our t-SNE analysis revealed distinct expression patterns between VISTA and PD-1 in endogenous T subpopulations with unique phenotypic characteristics, suggesting a potential synergistic effect of these pathways in immune suppression. Combinatorial blockade of VISTA, PD-1, or CTLA-4 resulted in improved therapeutic efficacy for tumor clearance.[18 33] Overall, our findings confirm the non-redundant role of VISTA in controlling T-cell activation and response that is distinct from the PD-1 and CTLA-4 pathways.

Potential limitations of our study include the lack of understanding regarding the precise mechanisms by which VISTA and its ligands interact with endogenous T cells within the TME following CAR-T therapy. VISTA was found to act as a receptor on T cells for the galectin 9 and VSIG-3 ligands and as a ligand for the PSGL-1 receptor.[34–36] Though B-ALL was VISTA negative, expression of VISTA as a ligand on DC might contribute to DC-mediated T-cell response in TME following CAR-T therapy. Besides, the generalizability of endogenous T-cell activation within TME following CAR-T cell therapy in other hematopoietic malignancies such as B-NHL, or solid tumors has not been adequately validated. In the present study, data from B lymphoma and melanoma murine models confirmed the augmented endogenous T-cell responses induced by CAR-T cells. Furthermore, ample evidence indicated that tumor-reactive T cells or CAR-T cells produce IFN-γ, which exerts a broad impact on infiltrating immune cells and tumor cells, as well as exhibits strong bystander activity within the TME.[37 38] And it should be noted that the TME of B-NHL or solid tumors is relatively more stable and sealed compared with the half-opened TME in B-ALL. Previous studies have reported that IFN-γ overcomes PD-L1/PD-1 inhibitory effects to sustain or enhance CAR-T anti-solid tumor activities through inducing ICAM-1 expression.[38] Furthermore, IFN-γ can enhance immune function yet also promoting T-cell exhaustion through PD-L1. The dual role of IFN-γ signaling in cancer cells and immune cells establishes a regulatory relationship between the adaptive and innate immune systems within the TME.[39]

Acknowledgements We thank Professor Peng Li (Guangzhou Institute of Biomedicine and Health, Chinese Academy of Sciences) who kindly provided the plasmid of anti-CD19 CAR. We thank Professor Meng Zhou (Anhui Medical University) who kindly provided technical advice. We thank Professor Zhinan Yin (Jinan University) who kindly provided the IFN-γ$^{-/-}$ and IFN-γR1$^{-/-}$ mice. We also thank Professor Qing Zhang and Shishuo Sun (Cancer Institute, Xuzhou Medical University) who provided the hCAIX CAR-T treated hCAIX^{+} melanoma murine model.

Contributors KZ and KX conceived of experiments, analyzed data, wrote and revised the paper, and are responsible for the overall content as the guarantor. DT executed experiments, analyzed data and wrote the paper. LZ, FY and CR assisted in performing experiments. All authors listed have made a substantial, direct, and intellectual contribution to the work and approved it for publication.

Funding The study is supported by The Science and Technology Development Fund of Affiliated Hospital of Xuzhou Medical University (XYFY2021013), the Postgraduate Research & Practice Innovation Program of Jiangsu Province (KYCX23_2979), The medical science and technology innovation project of Xuzhou Health Commission (XWKYHT20230064), and The Science and Technology Plan Projects of Xuzhou (KC23246).

Competing interests No, there are no competing interests.

Patient consent for publication Not applicable.

Ethics approval Not applicable.

Provenance and peer review Not commissioned; externally peer reviewed.

Data availability statement All data relevant to the study are included in the article or uploaded as supplementary information. Not applicable.

Supplemental material This content has been supplied by the author(s). It has not been vetted by BMJ Publishing Group Limited (BMJ) and may not have been peer-reviewed. Any opinions or recommendations discussed are solely those of the author(s) and are not endorsed by BMJ. BMJ disclaims all liability and responsibility arising from any reliance placed on the content. Where the content includes any translated material, BMJ does not warrant the accuracy and reliability of the translations (including but not limited to local regulations, clinical guidelines, terminology, drug names and drug dosages), and is not responsible for any error and/or omissions arising from translation and adaptation or otherwise.

J Immunother Cancer: first published as 10.1136/jitc-2023-008364 on 25 June 2024. Downloaded from http://jitc.bmj.com/ on June 26, 2024 by Exeter Team. Protected by copyright.

Open access This is an open access article distributed in accordance with the Creative Commons Attribution Non Commercial (CC BY-NC 4.0) license, which permits others to distribute, remix, adapt, build upon this work non-commercially, and license their derivative works on different terms, provided the original work is properly cited, appropriate credit is given, any changes made indicated, and the use is non-commercial. See http://creativecommons.org/licenses/by-nc/4.0/.

ORCID iDs
Kailin Xu http://orcid.org/0000-0003-1375-1084
Kai Zhao http://orcid.org/0000-0003-1740-3239

REFERENCES

1 Schultz L, Mackall C. Driving CAR T cell translation forward. *Sci Transl Med* 2019;11:eaaw2127.
2 Cao J, Wang G, Cheng H, *et al*. Potent anti-leukemia activities of Humanized Cd19-targeted Chimeric antigen receptor T (CAR-T) cells in patients with Relapsed/refractory acute Lymphoblastic leukemia. *Am J Hematol* 2018;93:851–8.
3 Maude SL, Laetsch TW, Buechner J, *et al*. Tisagenlecleucel in children and young adults with B-cell Lymphoblastic leukemia. *N Engl J Med* 2018;378:439–48.
4 Shah BD, Ghobadi A, Oluwole OO, *et al*. KTE-X19 for Relapsed or refractory adult B-cell acute Lymphoblastic leukaemia: phase 2 results of the single-arm, open-label, Multicentre ZUMA-3 study. *Lancet* 2021;398:491–502.
5 Park JH, Rivière I, Gonen M, *et al*. Long-term follow-up of Cd19 CAR therapy in acute Lymphoblastic leukemia. *N Engl J Med* 2018;378:449–59.
6 Cappell KM, Kochenderfer JN. Long-term outcomes following CAR T cell therapy: what we know so far. *Nat Rev Clin Oncol* 2023;20:359–71.
7 Xu X, Sun Q, Liang X, *et al*. Mechanisms of relapse after Cd19 CAR T-cell therapy for acute Lymphoblastic leukemia and its prevention and treatment strategies. *Front Immunol* 2019;10:2664.
8 Orlando EJ, Han X, Tribouley C, *et al*. Genetic mechanisms of target antigen loss in Car19 therapy of acute Lymphoblastic leukemia. *Nat Med* 2018;24:1504–6.
9 Fischer J, Paret C, El Malki K, *et al*. Cd19 Isoforms enabling resistance to CART-19 Immunotherapy are expressed in B-ALL patients at initial diagnosis. *J Immunother* 2017;40:187–95.
10 Asnani M, Hayer KE, Naqvi AS, *et al*. Retention of Cd19 Intron 2 contributes to CART-19 resistance in Leukemias with Subclonal Frameshift mutations in Cd19. *Leukemia* 2020;34:1202–7.
11 Shah NN, Fry TJ. Mechanisms of resistance to CAR T cell therapy. *Nat Rev Clin Oncol* 2019;16:372–85.
12 Zhao K, Ren C, Tang D, *et al*. The altering cellular components and function in tumor Microenvironment during Remissive and Relapsed stages of anti-Cd19 CAR T-cell treated lymphoma mice. *Front Immunol* 2023;14:1101769.
13 Scholler N, Perbost R, Locke FL, *et al*. Tumor immune Contexture is a determinant of anti-Cd19 CAR T cell efficacy in large B cell lymphoma. *Nat Med* 2022;28:1872–82.
14 Boulch M, Cazaux M, Loe-Mie Y, *et al*. A cross-talk between CAR T cell Subsets and the tumor Microenvironment is essential for sustained cytotoxic activity. *Sci Immunol* 2021;6:eabd4344.
15 Wang L, Rubinstein R, Lines JL, *et al*. VISTA, a novel Mouse IG Superfamily ligand that negatively regulates T cell responses. *J Exp Med* 2011;208:577–92.
16 ElTanbouly MA, Zhao Y, Nowak E, *et al*. VISTA is a Checkpoint regulator for Naïve T cell quiescence and peripheral tolerance. *Science* 2020;367:eaay0524.
17 Le Mercier I, Chen W, Lines JL, *et al*. VISTA regulates the development of protective antitumor immunity. *Cancer Res* 2014;74:1933–44.
18 Kondo Y, Ohno T, Nishii N, *et al*. Differential contribution of three immune Checkpoint (VISTA, CTLA-4, PD-1) pathways to antitumor responses against squamous cell carcinoma. *Oral Oncol* 2016;57:54–60.
19 Hosseinkhani N, Derakhshani A, Shadbad MA, *et al*. The role of V-domain IG Suppressor of T cell activation (VISTA) in cancer therapy: lessons learned and the road ahead. *Front Immunol* 2021;12:676181.
20 Gao J, Ward JF, Pettaway CA, *et al*. VISTA is an inhibitory immune Checkpoint that is increased after Ipilimumab therapy in patients with prostate cancer. *Nat Med* 2017;23:551–5.
21 Braumüller H, Wieder T, Brenner E, *et al*. T-Helper-1-cell Cytokines drive cancer into Senescence. *Nature* 2013;494:361–5.
22 Kotredes KP, Gamero AM. Interferons as Inducers of apoptosis in malignant cells. *Journal of Interferon & Cytokine Research* 2013;33:162–70.
23 Alizadeh D, Wong RA, Gholamin S, *et al*. Ifngamma is critical for CAR T cell-mediated myeloid activation and induction of endogenous immunity. *Cancer Discov* 2021;11:2248–65.
24 Spear P, Barber A, Rynda-Apple A, *et al*. Chimeric antigen receptor T cells shape myeloid cell function within the tumor Microenvironment through IFN-gamma and GM-CSF. *J Immunol* 2012;188:6389–98.
25 Lindo L, Wilkinson LH, Hay KA. Befriending the hostile tumor Microenvironment in CAR T-cell therapy. *Front Immunol* 2020;11:618387.
26 Jain MD, Zhao H, Wang X, *et al*. Tumor interferon signaling and suppressive myeloid cells are associated with CAR T-cell failure in large B-cell lymphoma. *Blood* 2021;137:2621–33.
27 Strati P, Neelapu SS. CAR-T failure: beyond antigen loss and T cells. *Blood* 2021;137:2567–8.
28 Stenger D, Stief TA, Kaeuferle T, *et al*. Endogenous TCR promotes in vivo persistence of Cd19-CAR-T cells compared to a CRISPR/Cas9-mediated TCR knockout CAR. *Blood* 2020;136:1407–18.
29 Xu W, Hiếu T, Malarkannan S, *et al*. The structure, expression, and Multifaceted role of immune-Checkpoint protein VISTA as a critical regulator of anti-tumor immunity, Autoimmunity, and inflammation. *Cell Mol Immunol* 2018;15:438–46.
30 Wang L, Jia B, Claxton DF, *et al*. VISTA is highly expressed on Mdscs and mediates an inhibition of T cell response in patients with AML. *OncoImmunology* 2018;7:e1469594.
31 Xu W, Dong J, Zheng Y, *et al*. Immune-Checkpoint protein VISTA regulates antitumor immunity by controlling myeloid cell–mediated inflammation and immunosuppression. *Cancer Immunol Res* 2019;7:1497–510.
32 Doroshow DB, Bhalla S, Beasley MB, *et al*. PD-L1 as a biomarker of response to immune-Checkpoint inhibitors. *Nat Rev Clin Oncol* 2021;18:345–62.
33 Liu J, Yuan Y, Chen W, *et al*. Immune-Checkpoint proteins VISTA and PD-1 Nonredundantly regulate murine T-cell responses. *Proc Natl Acad Sci USA* 2015;112:6682–7.
34 Johnston RJ, Su LJ, Pinckney J, *et al*. VISTA is an acidic pH-selective ligand for PSGL-1. *Nature* 2019;574:565–70.
35 Wang J, Wu G, Manick B, *et al*. VSIG-3 as a ligand of VISTA inhibits human T-cell function. *Immunology* 2019;156:74–85.
36 Yasinska IM, Meyer NH, Schlichtner S, *et al*. Ligand-receptor interactions of Galectin-9 and VISTA suppress human T lymphocyte cytotoxic activity. *Front Immunol* 2020;11:580557.
37 Thibaut R, Bost P, Milo I, *et al*. Bystander IFN-gamma activity promotes widespread and sustained cytokine signaling altering the tumor Microenvironment. *Nat Cancer* 2020;1:302–14.
38 Dong E, Yue X-Z, Shui L, *et al*. IFN-gamma surmounts PD-L1/Pd1 inhibition to CAR-T cell therapy by Upregulating ICAM-1 on tumor cells. *Signal Transduct Target Ther* 2021;6:20.
39 Benci JL, Johnson LR, Choa R, *et al*. Opposing functions of interferon coordinate adaptive and innate immune responses to cancer immune Checkpoint blockade. *Cell* 2019;178:933–48.

J Immunother Cancer: first published as 10.1136/jitc-2023-008364 on 25 June 2024. Downloaded from http://jitc.bmj.com/ on June 26, 2024 by Exeter Team. Protected by copyright.